

Temporal and Spatial Variation Characteristics of Rill Erosion and Hydrodynamic Parameters on Loessial Hillslope

Qin Chao¹ Wu Hongyan¹ Zheng Fenli^{1,2} Xu Ximeng¹ Bian Feng³

(1. State Key Laboratory of Soil Erosion and Dryland Farming on Loess Plateau, Institute of Soil and Water Conservation, Northwest A&F University, Yangling, Shaanxi 712100, China

2. Institute of Soil and Water Conservation, Chinese Academy of Sciences, Ministry of Water Resources, Yangling, Shaanxi 712100, China

3. College of Natural Resources and Environment, Northwest A&F University, Yangling, Shaanxi 712100, China)

Abstract: Rill erosion rate and hydrodynamic parameters present evident spatial and temporal variation characteristics during rill development process on hillslopes. Based on 3D laser scanning technique (LiDAR) and intermittent simulated rainfall experiments, high-precision DEMs were extracted. Temporal and spatial variations of rill erosion and hydrodynamic parameters at different rill development stages on loessial hillslope were analyzed. Results showed that the maximum values of rill erosion rate and hillslope erosion rate occurred at the rill deep cutting dominated stage, while the minimum values of them occurred at the rill headcut dominated stage. Rill erosion rates and hillslope erosion rates were increased at first and then tended to be steady and fluctuated in a certain range with rainfall duration. Hillslope erosion rates reached steady state earlier than rill erosion rates. Rill erosion rates and hillslope erosion rates under 90 mm/h rainfall intensity reached steady states earlier than those under 60 mm/h rainfall intensity. Rill erosion rates were first increased and then decreased along hillslope and showed parabola trend. The maximum values of rill erosion rate occurred at the hillslope lengths of 6 m and 7 m. Shear stress, stream power and unit stream power under 90 mm/h rainfall intensity were 1.3, 1.1 and 1.4 times as those under 60 mm/h rainfall intensity. Hydrodynamic parameters of overland flow and rill flow showed different variation trends with the increase of rainfall duration. Shear stress, stream power and unit stream power were increased with fluctuations of unit slope length under two rainfall intensities. It showed strong positive linear correlation between rill erosion per unit width and three hydrodynamic parameters. The critical values of shear stress, stream power and unit stream power reached the maximum values at initial phase of rill development.

Key words: rill erosion; 3D laser scanning technique; spatial and temporal variation; critical hydrodynamic parameters; loessial hillslope

0 Introduction

Rill erosion is one of the main erosion types of sloping croplands, and it is also the main cause of soil and nutrient loss. In rill erosion dominant area, rill erosion accounts for approximately 70% of the total soil loss^[1-2]. Once rill occurs on hillslope, soil erosion pattern changes from sheet erosion to rill erosion. The erosivity and transport capacity of concentrated rill flow are much larger than those of raindrop impact and sheet flow, which lead to significant increase of hillslope erosion^[3].

Many researches have focused on rill erosion and gained many achievements on rill erosion process^[4-5],

morphology^[6-7], affecting factors^[2-3] and hydrodynamic mechanism^[5, 8-9]. Recent studies reveals that the differences between rill erosion and other channel erosion are rill erosion always couples with severe soil loss and rill morphology changes rapidly^[10]. The counteraction effects of rill morphology on hillslope soil loss add the uncertainty of three main processes of rill development: rill head advance, rill bed deep cut and rill wall collapse. Shear stress is the main driven factor that cause rill bed deep cut^[10]. Shear stress and stream power are important hydrodynamic parameters of concentrated rill flow^[11-13]. Rill erosion is estimated by shear stress in WEPP model^[14]. Other researches indicated that

stream power is more accurate on estimating rill erosion than shear stress. However, recent studies mainly focused on the whole process of rill development, few distinguished the temporal and spatial variations of overland flow hydrodynamic parameters at different dominant erosion process of rill development.

On the other hand, limited by technical condition, rill survey with steel ruler^[6] and needle board technique^[7] are two recently used methods to research rill erosion. However, DEMs extracted from these data are often low precision. As a result, the temporal and spatial variations of rill development and the correlation between rill erosion rate and hydrodynamic parameters can hardly be well explored. In order to collect the precise rill erosion data in this study, 3D laser scanning technique (LiDAR) was applied for about every 10 min to get the information of hillslope elevation. At the active stage of rill development, the scanning interval was shortened to get more precise data. Based on 3D laser scanning technique and intermittent simulated rainfall experiments, high-precision DEMs were extracted to analyze rill erosion. Temporal and spatial variations of rill erosion rate and hydrodynamic parameters and their correlations at different rill development process on loessial hillslope were analyzed. It aims to provide theoretical basis for building hillslope soil erosion prediction model.

1 Materials and methods

1.1 Experimental materials

The study was conducted in the rainfall simulation laboratory at the State Key Laboratory of Soil Erosion and Dryland Farming on the Loess Plateau in Yangling City, China. A down pointing rainfall simulator system was used to apply rainfall. The raindrops fall from 18 m above the soil surface. The simulated rainfall was similar to natural rainfall regarding the raindrop size distribution, kinetic energy, and uniformity ($> 80\%$)^[15]. A soil box with 10.0 m-long, 1.5 m-wide and 0.5 m-deep was used in this study. Drainage holes (2 cm grid spacing) at the soil box bottom were used for drainage. The soil used in this study was loess which was collected at a well-drained site in Ansai Town (36°45'N, 109°11'E), which is located in the hilly gullied region of the Loess Plateau in Shaanxi Province, Northwest China. The soil texture was

28.3% sand, 58.1% silt, 13.6% clay, and contained 5.9 g/kg soil organic matter.

1.2 Experimental design

Based on the erosive rainstorm properties, high-intensity and short-duration, on the Loess Plateau ($I_5 = 1.52$ mm/min, $I_{10} = 1.05$ mm/min, I_5 and I_{10} represent the maximum 5 min and 10 min rainfall intensity in one natural rain)^[16], the rainfall intensities in this study were set to 60 mm/h and 90 mm/h (1.0 mm/min and 1.5 mm/min) for each rain. Because 15° is the critical slope gradient for rill occurrence on the loessial hillslope, 15° slope gradient was used. In this study, four groups of rains (two replicates with two rainfall intensities) were applied. All the data showed in this paper were the average number of the two replicates.

1.3 Experimental procedure

(1) Before packing the soil box, the soil water content was determined and used to calculate how much soil was needed for packing. The soil box was filled from the bottom to the top with sand and soil material. Specifically, the lower 5 cm of the soil box was filled with sand to allow free drainage of excess water. A highly permeable cloth was used to separate the sand and soil layers. To simulate the loessial soil profile in the field, a 15 cm plough pan with a soil bulk density of 1.35 g/cm³ was packed above the sand layer, and a 20 cm tilled layer with a soil bulk density of 1.10 g/cm³ was packed above the plough pan, each in 5 cm increments. Each packed soil layer was lightly raked before the next layer for homogeneity. The amount of soil in each layer was kept as constant as possible to maintain a similar soil bulk density and a uniform spatial distribution. After packing, manual tillage on the soil bed was performed to a depth of approximately 20 cm to simulate the ploughing depth of the croplands.

(2) Before conducting each experiment, pre-rain was applied at an intensity of 30 mm/h until surface runoff occurred. The purpose of the pre-rain was to maintain consistent soil moisture, consolidate loose soil particles by raindrop compaction, and reduce the spatial variability of underlying soil conditions. A plastic sheet was used to cover the soil box surface to prevent evaporation and soil surface sealing during 24 h of soil water redistribution.

(3) Rainfall intensity was calibrated to target rainfall intensity. Relative error between actual rainfall intensity and target rainfall intensity should be less than 5%.

(4) Soil surface changes were carefully observed as soon as rainfall was applied. Initial runoff occurrence time and position were recorded. Runoff samples were collected continuously at the former period time of each experiment. Two min collecting interval was used to collect runoff samples after runoff rate reaching stable stage. During the experiment procedure, two typical rills and two inter-rill positions were selected at each unit slope length to measure flow velocity with dye tracing method. Measuring section length was 50 cm (30 cm was also applied if the length was insufficient). SX40-1 gauge pin (0.1 mm measuring resolution)^[17] was used to measure rill and inter-rill flow depth. All of the measuring was applied for two replicates.

(5) Rill morphology measurement. A Leica scan station 2, 3D laser scanner (Leica Geosystems Inc., Switzerland) was used to scan the hillslope surface during the interval of rainfall (about 10 min). Specifically, the 3D laser scanner was mounted on a triangular shelf bracket 4.5 m above the ground and 3.0 m in front of the soil box to reduce the shadowing of the rill wall. Point clouds (with the resolution of 2 mm × 2 mm) were acquired by the scanner to quantify surface changes. The whole scanning process lasted for about 4.5 min. High-resolution video was also recorded during the experiment process.

(6) After rainfall, runoff samples were left over night to settle so that the excess water could be poured out. The samples were then put in an oven at 105°C for 24 h. Then samples were weighed and used to calculate the amount of runoff and sediment.

1.4 Parameters calculation

Hillslope soil erosion process is the work of runoff and the process of runoff energy dissipation. Shear stress (τ), stream power (ω) and unit stream power (φ) were selected in this study to quantify spatial and temporal variations of hillslope erosion and rill erosion.

Shear stress is calculated according to Eq. (1)^[9]:

$$\tau = \gamma RJ \quad (1)$$

where τ is shear stress, Pa; γ is the gravity of water, g/cm³; R is hydraulic radius, cm; J is hydraulic

slope, m/m, it could be replaced by tangent value of the slope gradient^[18].

There is significant relationship between stream power and shear stress^[19]. Stream power is calculated by Eq. (2):

$$\omega = \tau V \quad (2)$$

where ω is stream power, N/(cm · s); V is cross section mean flow velocity, cm/s, it equals to the flow velocity measured by dye tracing method times parameter 0.75^[20].

YANG^[21] presented the concept of unit stream power according to the equation of sediment transport. MOORE et al.^[22] applied this equation to hillslope and rill erosion calculation. Unit stream power is calculated by Eq. (3):

$$\varphi = \frac{dy}{dt} = \frac{dx}{dt} \frac{dy}{dx} = VJ \quad (3)$$

where φ is unit stream power, cm/s.

1.5 Data processing

(1) After the experiment, a series of preprocessing operations (including coordinate transformation and matching) were accomplished in Cyclone 6.0. Denoising and interpolating of points were applied to avoid reflection of raindrops and rill wall shadowing. After preprocessing, point clouds were down sampled and X , Y , Z coordinate system attributes were set up. Finally, point clouds were exported with the .txt format.

(2) The exported point clouds data were then imported into ArcGIS 10.1 to construct digital elevation models (DEMs). Processes of constructing DEMs include x , y layer, Tin and Shape file establishment, spatial adjustment with editor, Tin reestablishment and DEM construction. The resolution of DEM was averaged to 5 mm × 5 mm raster grids. Rills were extracted from the DEMs by using the Arc Hydro Tool with flow accumulation and the main flow path module.

(3) Rill erosion was then calculated by volume differentials of two DEMs (before and after each rain) and soil bulk density.

2 Results and discussions

2.1 Hillslope erosion and rill erosion amount under different rainfall intensities

The dominant erosion processes varied at different rill development stages. Rill erosion processes were

divided into three sub-procedures as follows in this study: rill head advance dominant process appeared at the early stage of rill development, it lasted from headcut formation to the formation of disconnected and connected rill; rill bed deep cut dominant process appeared in the middle of rill development process, it lasted from the formation of constant rill flow to rill incised to the plough pan (rill depth of 20 cm); rill wall collapse dominant process appeared in the last phase of rill development when rill was incised into plough pan, rill depth was above 20 cm, rill bed deep cut rate decreased and rill widening rate increased.

Rill erosion rate, hillslope erosion rate and contribution of rill erosion to hillslope erosion were different because of different dominant erosion process at different stages of rill development. Tab. 1 shows that the rill head advance dominant process lasts 30 min under 90 mm/h rainfall intensity and it is 10 min shorter than that under 60 mm/h rainfall intensity; the rill bed deep cut dominant process lasts 30 min under 60 mm/h and 90 mm/h rainfall intensities; the rill wall collapse dominant process begins at 60 min of the rainfall under 90 mm/h rainfall intensity and it is 10 min earlier than that under 60 mm/h rainfall intensity. The results showed that, as the dominant erosion process changed from rill head advance dominated to rill wall collapse dominated, maximums of rill erosion rate and hillslope erosion rate under two rainfall intensities occurred at the rill bed deep cut dominated process while contribution of rill erosion to hillslope erosion showed an increasing trend. The main reasons for these phenomenon are as follows: ① Soil resistance was relatively weak on the middle and lower parts of the hillslope at the rill head advance dominant process, and namely, shear stress was greater than the

critical shear stress^[23]. Intermittent rill head was formed first, and gradually connected to form disconnected rills with the process of headward retreat. Then constant flow path and small watershed formed (Fig. 1a and Fig. 1d). The slope dissected degree was relatively low, inter-rill flow was dominated, runoff erosivity was smaller than that during the latter periods; and thus rill erosion rates were 8.3 kg/(m²·h) and 22.8 kg/(m²·h) under 60 mm/h and 90 mm/h rainfall intensities, respectively, which were respectively equivalent to 1/3 and 1/2 of the maximum rill erosion rate. Hillslope erosion rate and the contribution of rill erosion to hillslope erosion were also small. ② Rill bed deep cut dominant process with rill wall collapse was the most active stage of rill development. At this process, rill head advanced very close to the top of the hillslope, the slope dissected degree was greater, the velocity, energy, shear stress and stream power of rill flow increased and were greater than those of inter-rill flow, as a result, rills became deeper and rill flow became more constant. Though rill wall collapse at this stage, but rill widening was not the major factor that caused rill erosion increase (Fig. 1b and Fig. 1e). ③ Rill wall collapse dominant process was the last phase of rill development which was consistent with the results given by BRUNTON et al. on loessial hillslope in Canada^[23]. Due to the fact that rill head advance and deep cut process nearly stopped, the main source of sediment came from rill wall collapse (Fig. 1c and Fig. 1f). Inter-rill erosion caused by inter-rill flow was relatively small and thus the contribution of rill erosion to hillslope erosion was the largest during the whole process (more than 75% under 60 mm/h and 90 mm/h rainfall intensities). However, rill erosion rates and hillslope erosion rates

Tab. 1 Rill erosion rate, hillslope erosion rate and contribution of rill erosion to hillslope erosion at different dominant processes of rill development

Rainfall intensity/ (mm·h ⁻¹)	Dominant erosion process	Rainfall duration/ min	Rill erosion rate/(kg·m ⁻² ·h ⁻¹)	Hillslope erosion rate/ (kg·m ⁻² ·h ⁻¹)	Contribution of rill erosion to hillslope erosion/%
60	Rill head advance	0 ~ 40	8.3	22.4	37.1
	Rill bed deep cut	40 ~ 70	24.3	31.9	76.2
	Rill wall collapse	70 ~ 90	24.2	31.6	76.5
90	Rill head advance	0 ~ 30	22.8	42.7	53.4
	Rill bed deep cut	30 ~ 60	48.0	61.6	77.8
	Rill wall collapse	60 ~ 90	40.8	50.7	80.5

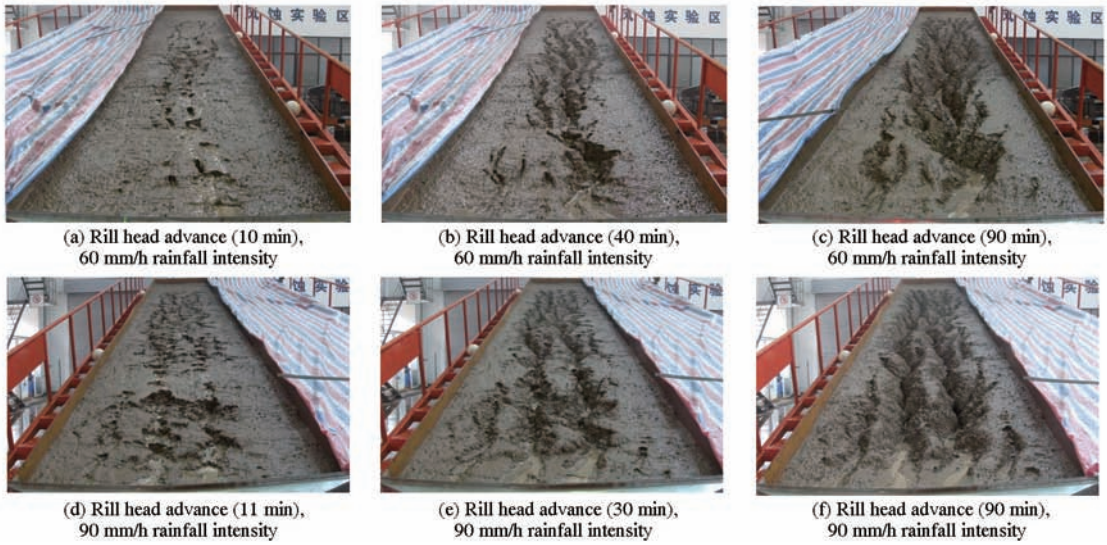


Fig. 1 Dominated erosion patterns at different stages of rill development process

were smaller than those at rill bed deep cut dominant process because rill wall collapse has the characteristics of uncertainty and abruptness.

2.2 Spatial and temporal variations of rill erosion

2.2.1 Spatial variations of rill erosion

The amount of hillslope erosion were 621.3 kg and 1 162.5 kg, the amount of rill erosion were 386.3 kg and 837.0 kg, and the contribution of rill erosion to hillslope erosion were 62.2% and 72.0% under 60 mm/h and 90 mm/h rainfall intensities, respectively (Fig. 2). Hillslope erosion rates reached steady state earlier than rill erosion rates under the same rainfall intensity. Larger rainfall intensity made hillslope erosion rates and rill erosion rates reach steady state earlier. Rill erosion rates and hillslope erosion rates needed 40 min and 60 min to reach steady state under 60 mm/h rainfall intensity and then fluctuated between 30.6 ~ 32.9 kg/(m²·h) and 23.6 ~ 26.8 kg/(m²·h), respectively. Rill erosion rates and hillslope erosion rates needed 30 min and 40 min to reach steady state

under 90 mm/h rainfall intensity, 10 min and 20 min earlier than those under 60 mm/h rainfall intensity and then fluctuated between 47.7 ~ 67.0 kg/(m²·h) and 37.7 ~ 45.7 kg/(m²·h), respectively. The results was consistent with previous researches which showed that rill development reached steady stage earlier with the increase of rainfall intensity^[24]. This could be attributed to that raindrop energy and flow confluence intensity were greater at the 90 mm/h rainfall intensity, raindrop splash and runoff erosion were more serious, slope erosion process developed faster and rill development reached steady stage earlier, namely, the time reaching rill wall collapse dominant process was earlier than that of 60 mm/h rainfall intensity. The contribution of rill erosion to hillslope erosion reached steady state earlier under 90 mm/h rainfall intensity, and it fluctuated between 72.6% ~ 81.5% under two rainfall intensities. This was consistent with previous research results on rill erosion dominant regions on the Loess Plateau which showed that the contribution of rill

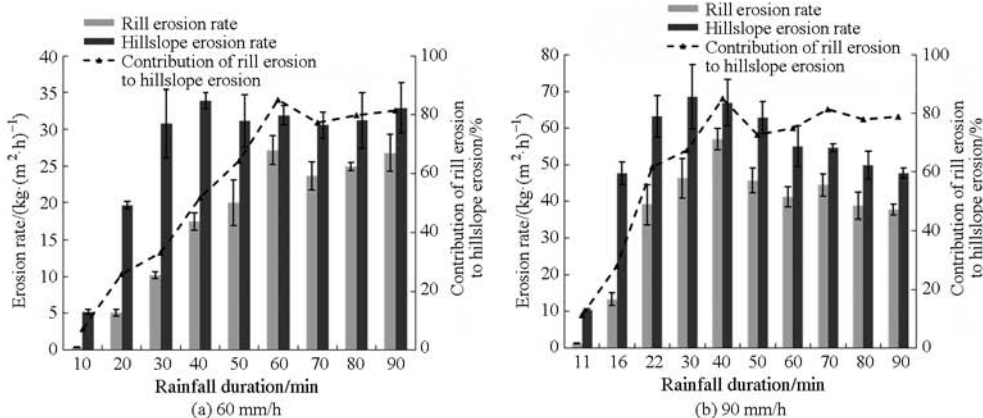
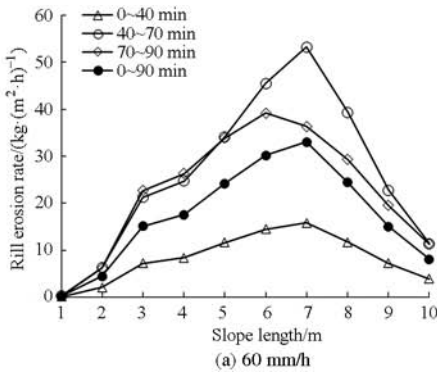


Fig. 2 Rill erosion rate, hillslope erosion rate and contribution of rill erosion to hillslope erosion with different rainfall durations

erosion to hillslope erosion was about 70%^[1-2].

2.2.2 Characteristics of rill erosion rate along hillslope

Rill erosion rates first increased, and then decreased along hillslope and showed parabola trend under two rainfall intensities (Fig. 3). Regarding different rill development process, maximums of rill erosion rate



occurred at the rill bed deep cut dominant process with rill wall collapse while minimums of rill erosion rate occurred at the rill head advance dominant process (Tab.1 and Fig.2). Regarding different slope positions, rill erosion rates at middle and down slope position were larger than those at other slope positions (Fig.3).

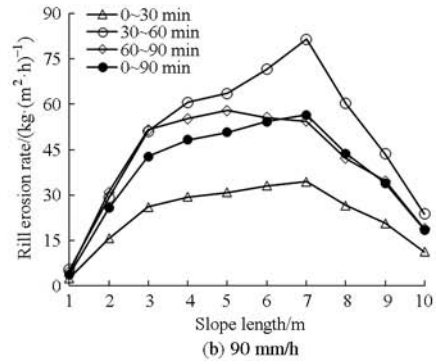


Fig. 3 Changes of rill erosion rate with unit slope length at different stages of rill development process

Trend lines of average rill erosion rate with unit slope length under 60 mm/h rainfall intensity distributed between trend lines of 0 ~ 40 min and 70 ~ 90 min rainfall durations. Maximum of rill erosion rate was 33.1 kg/(m²·h), occurred at the slope length of 7 m, and it was 3.3 times as the average value. This result was consistent with previous study which showed that the most serious erosion area located at middle and down slope position on the hillslope^[25-26]. At the early stage of rill development process (0 ~ 40 min, rill head advance dominated), changes of rill erosion rate with unit slope length were gentle. At the middle stage of rill development process (40 ~ 70 min, rill bed deep cut dominated with rill wall collapse), rill erosion rates at 5 ~ 8 m slope length were larger than those at other slope positions. Rills developed fast at this stage, and after that, rill development tended to be steady, some part of the main rill bed cut into plough pan.

Changes of rill erosion rate with unit slope length at different stages of rill development process under 90 mm/h rainfall intensity were similar with those of 60 mm/h rainfall intensity. The average rill erosion rate under 90 mm/h rainfall intensity was 1.8 ~ 2.8 times as that under 60 mm/h rainfall intensity. However, at the last rill development process (70 ~ 90 min), rill erosion rate decreased from 4 m slope length under 90 mm/h rainfall intensity, while decreased from 6 m slope length under 60 mm/h

rainfall intensity.

The slope length of 1 ~ 7 m was dominated by erosion-transport process under two rainfall intensities based on 3D laser scanning data. Shear stress and stream power on the upper slope position were less than those at middle and down slope position on the hillslope limited by slope length (Fig.4). As a result, rill erosion rate showed the same trend. On the other hand, inter-rill erosion was dominated at the slope length of 1 m, which led to the average rill erosion rates were 0.2 kg/(m²·h) and 3.7 kg/(m²·h) under 60 mm/h and 90 mm/h rainfall intensities, respectively (Fig.3). Contributing area, runoff erosivity, stream power and unit stream power increased with the increase of slope length (Fig.4). Rill erosion rate gradually decreased after it reaching maximum. Hillslope erosion, transportation and deposition existed at the same time while deposition process dominated at the slope length of 8 ~ 9 m, which was consistent with previous research results given by WU et al.^[26]. Rill erosion rate decreased significantly at the slope length of 10 m. The high-precision DEMs extracted from point clouds data showed that deposition was the dominant process at this slope length, and rills were wide and shallow, which were different from narrow and deep rills at upper and middle slope positions (Fig.1). The above results were similar to rill erosion-deposition process fulfilled by BRUNTON et al.^[23]

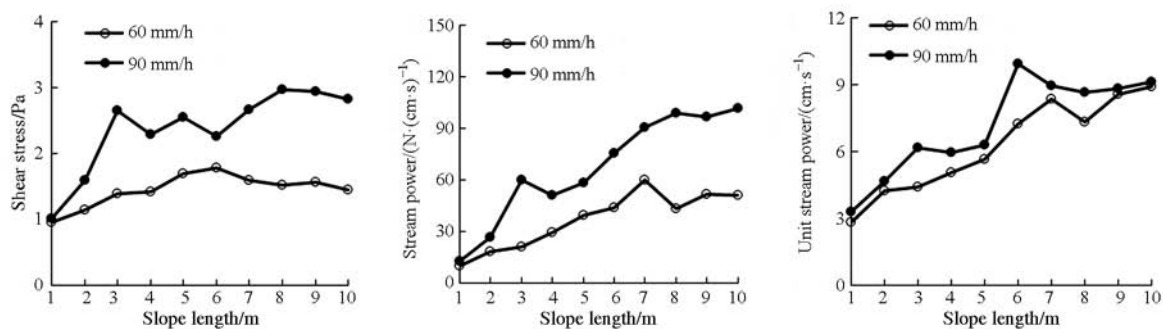


Fig. 4 Changes of shear stress, stream power and unit stream power with unit hillslope length

2.3 Spatial and temporal variations of hydrodynamic parameters

2.3.1 Spatial variations of hydrodynamic parameters

Shear stress, stream power and unit stream power under 90 mm/h rainfall intensity were 1.3, 1.1 and 1.4 times as those under 60 mm/h (Tab. 2). The average values of shear stress, stream power and unit stream power of the whole slope decreased under two rainfall intensities from the rill head advance dominant process to rill wall collapse dominant process at different stages of rill development process. The variations of three hydrodynamic parameters of rill and inter-rill flow were different at different stages of rill development process, which verified the results of changes of rill erosion process can significantly affect hydrodynamic characteristics^[27]. Specifically, hydrodynamic parameters of inter-rill flow decreased, while those of rill flow increased first and then

decreased with the increase of rainfall duration under two rainfall intensities. Main reasons were as follow:

① At the very early stage of rill development, hillslope was relatively integrated and overland flow was dominated by inter-rill flow. After that, runoff concentrated into rills, contributing area of inter-rill flow decreased which lead to inter-rill flow volume and flow velocity decreased rapidly. As a result, shear stress, stream power and unit stream power of the inter-rill decreased with the rainfall process. ② In contrast to inter-rill flow, rill flow hydrodynamic parameters increased as overland flow concentrated into rills. However, due to the uncertainty of rill wall collapse, soil blocks deposited in the rill channel led to rill flow velocity decreased and rill flow width and depth increased. As a result, hydrodynamic parameters of rill flow decreased at the rill wall collapse cut dominant process.

Tab. 2 Shear stress, stream power and unit stream power of inter-rill flow and rill flow at different stages of rill development process

Rainfall intensity/ (mm·h ⁻¹)	Dominant erosion process	Rainfall duration/min	Runoff type	τ /Pa	ω /(N·cm ⁻¹ ·s ⁻¹)	φ /(cm·s ⁻¹)
60	Rill head advance	0 ~ 40	Inter-rill	1.3	25.4	6.0
			Rill	2.1	63.5	7.9
	Rill bed deep cut	40 ~ 70	Inter-rill	1.0	13.5	3.4
			Rill	2.2	69.5	7.9
	Rill wall collapse	70 ~ 90	Inter-rill	0.8	12.3	3.1
			Rill	1.7	55.5	7.7
90	Rill head advance	0 ~ 30	Inter-rill	1.6	41.4	6.3
			Rill	2.8	85.9	8.5
	Rill bed deep cut	30 ~ 60	Inter-rill	1.2	16.9	3.9
			Rill	3.1	95.3	9.1
	Rill wall collapse	60 ~ 90	Inter-rill	1.1	15.4	3.6
			Rill	2.5	82.8	8.7

2.3.2 Hydrodynamic parameters characteristics along unit slope length

Shear stress, stream power and unit stream power showed an increasing trend along unit slope length

under two rainfall intensities (Fig. 4). Three hydrodynamic parameters showed obvious fluctuations under 90 mm/h rainfall intensity due to the uncertainty of rill development and severe scouring effects of rill

wall toe and rill head. The average scouring concave depth of rill head at the rill head advance dominant process was 3.5 cm under 90 mm/h rainfall intensity and it was 1.3 cm deeper than that under 60 mm/h rainfall intensity. The positive relationship between scouring concave depth of rill head and upslope inflow rate was also verified by WELLS et al.^[28]. The average scouring concave depth of rill wall toe at the rill wall collapse dominant process was 4.2 cm under 90 mm/h rainfall intensity and it was 1.5 cm deeper than that under 60 mm/h rainfall intensity. The larger scouring concave depth of rill wall toe resulted in high uncertainties of rill wall collapse and finally affected rill flow velocity and flow regime, which contributed to the variations of three hydrodynamic parameters along slope length. Rill head advance rate increased with the increase of scouring concave depth of rill head^[28]. Variations of three hydrodynamic parameters with unit slope length were consistent with variations of rill erosion rates at the slope length of 0 ~ 7 m. Rill erosion rate increased with the increase of shear stress, stream power and unit stream power. However, at the slope length of 7 ~ 10 m, variations of rill erosion rates showed opposite trend to three hydrodynamic parameters. Rill erosion rate decreased with the increase of three hydrodynamic parameters, which could be attributed to the changes of runoff transport capacity and erosion process (changed from erosion dominant to deposition dominant)^[23].

2.4 Correlations between rill erosion and hydrodynamic parameters

Equations between rill erosion per unit width and three hydrodynamic parameters (shear stress, stream power and unit stream power) were established at different stages of rill development process under two rainfall intensities. Only rill erosion per unit width and three hydrodynamic parameters at the slope length of 2 ~ 7 m were selected due to that sheet erosion was

dominated at the slope length of 1 m and the slope length of 7 ~ 10 m was the deposition area. Tab. 3 indicates that rill erosion per unit width D_c showed a linear correlation with three hydrodynamic parameters and the correlation coefficient was more than 0.6. The maximum of the monomial coefficient occurred at the rill bed deep cut dominant process, which was consistent with that both of the rill erosion rate and hillslope erosion rate reached the maximum at this process. When rill erosion per unit width $D_c = 0$, the corresponding constant term was the critical shear stress, stream power and unit stream power (Tab. 3). The critical shear stress, stream power and unit stream power were 0.748 Pa, 1.319 N/(cm · s) and 1.504 cm/s at the rill head advance dominant process, respectively. The critical shear stress, stream power and unit stream power decreased with the rill development process; and three critical hydrodynamic parameters at the rill wall collapse dominant process were 48.6%, 62.6% and 50.1% of those at the rill head advance dominant process. The above phenomenon could be attributed to: ① Pre-rain facilitated soil crust form and large flow energy was needed to cause soil erosion, which was consistent with previous research results on the black soil^[29]. ② At the second stage, soil crust was broken and rill flow dominated overland flow, flow rate and flow velocity increased which led to critical shear stress, stream power and unit stream power decrease. ③ At the third stage, the main source of sediment yield was rill wall collapse. Due to the vortex effect of rill flow, rill toe was scoured and formed diamond cross section at the middle and down slope position (Fig. 1f). Rill wall collapsed when rill wall self-gravity was larger than cohesive force of soil particles. The result corresponded with that given by WELLS et al. in Mississippi region of America^[30]. Rill wall collapse was the result of combined effects of water erosion and gravity

Tab.3 Fitted equations between rill erosion per unit width and hydrodynamic parameters at different stages of rill development process

Dominant erosion process	τ			ω			φ		
	Equations	Sample number	R^2	Equations	Sample number	R^2	Equations	Sample number	R^2
Rill head advance	$D_c = 54.97(\tau - 0.748)$	14	0.85	$D_c = 1.262(\omega - 1.319)$	14	0.68	$D_c = 11.29(\varphi - 0.015)$	14	0.63
Rill bed deep cut	$D_c = 82.61(\tau - 0.675)$	14	0.82	$D_c = 2.131(\omega - 1.075)$	14	0.82	$D_c = 21.01(\varphi - 0.012)$	14	0.62
Rill wall collapse	$D_c = 50.44(\tau - 0.364)$	14	0.66	$D_c = 1.763(\omega - 0.827)$	14	0.74	$D_c = 14.12(\varphi - 0.007)$	14	0.63

erosion, the relationship between rill erosion per unit width and hydrodynamic parameters decreased which led to the decrease of critical shear stress, stream power and unit stream power.

3 Conclusions

(1) Under the rainfall intensity of 90 mm/h, hillslope erosion, rill erosion and contribution of rill erosion to hillslope erosion were 1.9, 2.2 and 1.2 times as those under 60 mm/h rainfall intensity. The time of reaching maximum of hillslope erosion, rill erosion and contribution of rill erosion to hillslope erosion under 90 mm/h rainfall intensity was earlier than those under 60 mm/h rainfall intensity.

(2) The maximum of rill erosion rate and hillslope erosion rate occurred at rill bed deep cut dominant process. The minimum of rill erosion rate and hillslope erosion rate occurred at rill head advance dominant process. Regarding different slope positions, rill erosion rate increased first and then decreased along slope length which showed parabola trend. Rill erosion rates at middle and down slope position were larger than those at other slope positions.

(3) Under the rainfall intensity of 90 mm/h, shear stress, stream power and unit stream power were 1.3, 1.1 and 1.4 times as those under 60 mm/h rainfall intensity. Hydrodynamic parameters of inter-rill flow decreased with rill development. Hydrodynamic parameters of rill flow increased first and then decreased with rill development.

(4) Critical shear stress, critical stream power and critical unit stream power that cause hillslope erosion occur reached maximum at the rill head advance dominant process. Rill wall collapse was the dominant erosion process at the final stage of rill development, critical shear stress, critical stream power and critical unit stream power reached minimum.

References

[1] ZHU Xianmo. Main water erosion types and their related factors in the Loess Plateau [J]. *Bulletin of Soil and Water Conservation*, 1982(1): 1–9. (in Chinese)

[2] ZHENG Fenli, TANG Keli, ZHOU Peihua. Study on factors affecting rill erosion on cultivated slope land [J]. *Acta Pedologica Sinica*, 1989, 26(2): 109–116. (in Chinese)

[3] LI Junlan, CAI Qiangguo, SUN Liying, et al. Reviewing

on factors and critical conditions of rill erosion [J]. *Process in Geography*, 2010, 29(11): 1319–1325. (in Chinese)

- [4] ZHENG F L, TANG K L. Rill erosion process on steep slope land of the Loess Plateau [J]. *International Journal of Sediment Research*, 1997, 12(1): 52–59.
- [5] ELLIOT W J, LAFLEN J M. A process-based rill erosion model [J]. *Transactions of the ASAE*, 1993, 36(1): 65–72.
- [6] SHEN Haiou, ZHENG Fenli, WEN Leilei, et al. Effects of rainfall intensity and slope gradient on rill morphological characteristics [J]. *Transactions of the Chinese Society for Agricultural Machinery*, 2015, 46(7): 162–170. (in Chinese)
- [7] ZHANG Yongdong, WU Shufang, FENG Hao, et al. Experimental study of rill dynamic development process and its critical dynamic conditions on loess slope [J]. *Journal of Sediment Research*, 2013(2): 25–32. (in Chinese)
- [8] LI Peng, LI Zhanbin, ZHENG Liangyong. Indoor experiment of characteristics of runoff erosion in loess steep slope [J]. *Transactions of the CSAE*, 2005, 21(7): 42–45. (in Chinese)
- [9] FOSTER G R, HUGGINS L F, MEYER L D. A laboratory study of rill hydraulics: II. shear stress relationships [J]. *Transactions of the ASAE*, 1984, 27(3): 797–804.
- [10] HAN Peng, NI Jinren, LI Tianhong. Headcut and bank landslip in rill evolution [J]. *Journal of Basic Science and Engineering*, 2002, 10(2): 115–125. (in Chinese)
- [11] MEYER L D, FORSTER G R, NIKOLOVE S. Effect of flow rate and canopy on rill erosion [J]. *Transactions of the ASAE*, 1975, 18(5): 905–911.
- [12] LYLE W M, SMERDEN E T. Relation of compaction and other soil prosperities to erosion resistance of soils [J]. *Transactions of ASAE*, 1965, 8: 419–422.
- [13] NEARING M A, BRADFORD J M, PARKER S C. Soil detachment by shallow flow at low slopes [J]. *Soil Science Society of American Journal*, 1991, 55(2): 339–344.
- [14] NEARING M A, FOSTER G R, LANE L J, et al. A process based soil erosion model for USDA—water erosion prediction project technology [J]. *Transactions of the ASAE*, 1989, 32(5): 1587–1593.
- [15] ZHENG Fenli, ZHAO Jun. Introduction of the artificial rainfall simulation hall and simulated rainfall equipment [J]. *Research of Soil and Water Conservation*, 2004, 11(4): 177–178. (in Chinese)
- [16] ZHOU Peihua, WANG Zhanli. Soil erosion storm rainfall standard in the Loess Plateau [J]. *Bulletin of*

- Soil and Water Conservation, 1987, 7(1): 38 - 44. (in Chinese)
- [17] SHI Mingxin, LI Taotao, WU Bingxiao, et al. Influences of surface roughness on overland flow hydraulic characteristics [J]. Journal of Sediment Research, 2015(4): 59 - 65. (in Chinese)
- [18] ZHU J C, GANTZER C J, ANDERSON S H, et al. Simulated small-channel bed scour and head cut erosion rates compared [J]. Soil Science Society of America Journal, 1995, 59(1): 211 - 218.
- [19] BAGNOLD R A. An approach to the sediment transport problem for general physics[M]. Washington: United States Government Printing Office, 1966: 5.
- [20] SHEN Haiou, ZHENG Fenli, WEN Leilei, et al. Effects of raindrop impact on rill erosion characteristics on Loess Hillslope [J]. Transactions of the Chinese Society for Agricultural Machinery, 2015, 46(8): 104 - 112, 89. (in Chinese)
- [21] YANG C T. Incipient motion and sediment transport [J]. Journal of the Hydraulics Division, 1973, 99(10): 1679 - 1704.
- [22] MOORE I D, BURCH G J. Sediment transport capacity of sheet and rill flow: application of unit stream power theory[J]. Water Resources Research, 1986, 22(8): 1350 - 1360.
- [23] BRUNTON D A, BRYAN R B. Rill network development and sediment budgets [J]. Earth Surface Processes and Landforms, 2000, 25(7): 783 - 800.
- [24] BERGER C, SCHULZE M, RIEKE-ZAPP D, et al. Rill development and soil erosion: a laboratory study of slope and rainfall intensity [J]. Earth Surface Processes and Landforms, 2010, 35(12): 1456 - 1467.
- [25] QIN Chao, ZHENG Fenli, XU Ximeng, et al. Effects of maize straw buffer in preventing rill erosion on loess slope [J]. Science of Soil and Water Conservation, 2015, 13(1): 35 - 42. (in Chinese)
- [26] WU Pute, ZHOU Peihua, WU Chunlong, et al. Research on the spatial distribution characteristics of slope rill erosion [J]. Research of Soil and Water Conservation, 1997, 4(2): 47 - 56. (in Chinese)
- [27] WEN Leilei, ZHENG Fenli, SHEN Haiou, et al. Effects of corn straw mulch buffer in the gully head on gully erosion of sloping cropland in the black soil region of northeast China [J]. Journal of Sediment Research, 2014(6): 73 - 80. (in Chinese)
- [28] WELLS R R, BENNETT S J, ALONSO C V. Modulation of headcut soil erosion in rills due to upstream sediment loads [J]. Water Resources Research, 2010, 46(12): 1 - 16.
- [29] AN J, ZHENG F L, LU J, et al. Investigating the role of raindrop impact on hydrodynamic mechanism of soil erosion under simulated rainfall conditions [J]. Soil Science, 2012, 177(8): 517 - 526.
- [30] WELLS R R, MOMM H G, RIGBY J R, et al. An empirical investigation of gully widening rates in upland concentrated flows [J]. CATENA, 2013, 101: 114 - 121.

黄土坡面细沟侵蚀及水动力学参数的时空变化特征

覃超¹ 吴红艳¹ 郑粉莉^{1,2} 徐锡蒙¹ 边锋³

(1. 西北农林科技大学水土保持研究所高原土壤侵蚀与旱地农业国家重点实验室, 陕西杨凌 712100;

2. 中国科学院水利部水土保持研究所, 陕西杨凌 712100; 3. 西北农林科技大学资源环境学院, 陕西杨凌 712100)

摘要: 坡面细沟侵蚀速率和水动力学参数在坡面细沟发育过程中存在明显的时空变化。基于间歇性人工模拟降雨和三维激光扫描技术提取的高精度 DEM, 分析了黄土坡面细沟发育不同主导过程中细沟侵蚀和水动力学参数的时空分布规律。结果表明, 细沟侵蚀速率和总侵蚀速率的最大值出现在以细沟沟底下切侵蚀为主的细沟发育活跃期, 最小值出现在以沟头溯源侵蚀为主的细沟发育初期。细沟侵蚀速率与总侵蚀速率随降雨历时的变化皆呈先上升后趋于稳定, 并在一定范围内波动的变化趋势, 且总侵蚀速率早于细沟侵蚀速率达到稳定。细沟侵蚀量随单位斜坡长呈先上升后下降的抛物线形式分布, 细沟侵蚀速率的最大值出现在坡面中下部。90 mm/h 降雨强度下径流剪切力、径流功率和单位径流功率分别是 60 mm/h 降雨强度下的 1.3、1.1、1.4 倍。细沟间水流和细沟流的水动力学参数随降雨历时的增加呈不同的变化趋势。两种降雨强度下, 径流剪切力、径流功率和单位径流功率随单位坡长的分布均呈波动上升趋势。单宽细沟侵蚀量与水动力学参数之间呈线性正相关关系, 细沟发育初期坡面侵蚀发生的临界径流剪切力、临界径流功率和临界单位径流功率最大。

关键词: 细沟侵蚀; 三维激光扫描技术; 时空变化; 临界水动力学参数; 黄土坡面

中图分类号: S157 **文献标识码:** A **文章编号:** 1000-1298(2016)08-0146-09

Temporal and Spatial Variation Characteristics of Rill Erosion and Hydrodynamic Parameters on Loessial Hillslope

Qin Chao¹ Wu Hongyan¹ Zheng Fenli^{1,2} Xu Ximeng¹ Bian Feng³

(1. State Key Laboratory of Soil Erosion and Dryland Farming on Loess Plateau, Institute of Soil and Water Conservation, Northwest A&F University, Yangling, Shaanxi 712100, China

2. Institute of Soil and Water Conservation, Chinese Academy of Sciences, Ministry of Water Resources, Yangling, Shaanxi 712100, China

3. College of Natural Resources and Environment, Northwest A&F University, Yangling, Shaanxi 712100, China)

Abstract: Rill erosion rate and hydrodynamic parameters present evident spatial and temporal variation characteristics during rill development process on hillslopes. Based on 3D laser scanning technique (LiDAR) and intermittent simulated rainfall experiments, high-precision DEMs were extracted. Temporal and spatial variations of rill erosion and hydrodynamic parameters at different rill development stages on loessial hillslope were analyzed. Results showed that the maximum values of rill erosion rate and hillslope erosion rate occurred at the rill deep cutting dominated stage, while the minimum values of them occurred at the rill headcut dominated stage. Rill erosion rates and hillslope erosion rates were increased at first and then tended to be steady and fluctuated in a certain range with rainfall duration. Hillslope erosion rates reached steady state earlier than rill erosion rates. Rill erosion rates and hillslope erosion rates under 90 mm/h rainfall intensity reached steady states earlier than those under 60 mm/h rainfall intensity. Rill erosion rates were first increased and then decreased along hillslope and showed parabola trend. The

收稿日期: 2015-12-27 修回日期: 2016-02-02

基金项目: 国家自然科学基金项目(41271299)

作者简介: 覃超(1989—), 男, 博士生, 主要从事土壤侵蚀过程与机理研究, E-mail: glqinchao@nwsuaf.edu.cn

通信作者: 郑粉莉(1960—), 女, 教授, 博士生导师, 主要从事土壤侵蚀过程、预报和侵蚀环境效应评价研究, E-mail: flzh@ms.iswc.ac.cn

maximum values of rill erosion rate occurred at the hillslope lengths of 6 m and 7 m. Shear stress, stream power and unit stream power under 90 mm/h rainfall intensity were 1.3, 1.1 and 1.4 times as those under 60 mm/h rainfall intensity. Hydrodynamic parameters of overland flow and rill flow showed different variation trends with the increase of rainfall duration. Shear stress, stream power and unit stream power were increased with fluctuations of unit slope length under two rainfall intensities. It showed strong positive linear correlation between rill erosion per unit width and three hydrodynamic parameters. The critical values of shear stress, stream power and unit stream power reached the maximum values at initial phase of rill development.

Key words: rill erosion; 3D laser scanning technique; spatial and temporal variation; critical hydrodynamic parameters; loessial hillslope

引言

细沟侵蚀是坡耕地的主要侵蚀方式之一,也是坡耕地表土和养分流失的重要原因,在细沟侵蚀区,细沟侵蚀量占坡面总侵蚀量的 70% 左右^[1-2]。坡面上一旦产生细沟,坡面侵蚀方式即由片蚀转变为细沟侵蚀,细沟内股流的侵蚀力与挟沙力远大于雨滴打击和坡面薄层水流所具有的侵蚀力和挟沙力,从而导致坡面侵蚀量显著增加^[3]。

国内、外学者对细沟侵蚀进行了大量研究,在细沟侵蚀过程^[4-5]、细沟形态^[6-7]、细沟侵蚀影响因素^[2-3]和细沟侵蚀水动力学机理^[5, 8-9]等方面取得了丰富的研究成果。已有研究表明,细沟侵蚀与其它沟道侵蚀的区别在于,细沟的发育过程始终伴随着强烈的侵蚀产沙,细沟形态变化迅速^[10],而变化的细沟形态又反作用于坡面侵蚀产沙过程,增加了细沟发育过程中沟头溯源侵蚀、沟底下切侵蚀和沟壁崩塌侵蚀三者之间的复杂性和不确定性。研究还表明,水流剪切力是细沟沟底下切的主要驱动因子^[10],径流剪切力和径流功率是细沟侵蚀水动力学的重要参数^[11-13]。WEPP 模型用径流剪切力估算细沟侵蚀量^[14],也有研究指出基于径流功率估算的细沟侵蚀量较径流剪切力更为准确^[5]。然而,现有研究的时间尺度多为细沟发育的整个过程,较少区分细沟发育不同主导过程中坡面流的水动力学参数在时间和空间尺度上的变化。

另一方面,受技术条件限制,现有研究多利用测尺法^[6]和测针板法^[7]研究细沟侵蚀量,数据精度较低,难以获得高精度的 DEM。进而缺乏对细沟发育过程的时空变化分析,也不能很好地揭示细沟侵蚀速率与坡面流水动力学参数的关系。为精确获取坡面细沟侵蚀量,本研究在降雨过程中每隔约 10 min 用三维激光扫描技术(LiDAR)获取试验土槽坡面高程信息,并在细沟发育活跃期增加三维激光扫描的次数。用基于三维激光扫描获取的高精度 DEM 提取坡面细

沟侵蚀量数据,研究细沟侵蚀速率和坡面流水动力学参数的时空变化特征,进而分析细沟发育不同主导过程中细沟侵蚀速率和坡面流水动力学参数的关系,以期为坡面土壤侵蚀预报模型的建立提供理论依据。

1 材料与方 法

1.1 试验材料

试验在黄土高原土壤侵蚀与旱地农业国家重点实验室人工模拟降雨大厅进行。降雨设备为下喷式人工降雨装置,降雨高度 18 m,降雨均匀度大于 80%,雨滴直径和雨滴分布与天然降雨相似^[15]。试验土槽采用长 10.0 m、宽 3.0 m、深 0.5 m 的固定式液压升降钢槽,中间用钢板隔开,钢槽底部每 1 m 长均匀布置 4 个孔径为 2 cm 的排水孔以保证降雨试验过程中排水良好。供试土壤为黄土高原丘陵沟壑区安塞县的黄绵土,其中有机质质量比为 5.9 g/kg,黏粒、粉粒与砂粒分别占 13.6%、58.1% 和 28.3%,以上均为质量分数。

1.2 试验设计

根据黄土高原常见的短历时、高强度侵蚀性降雨标准^[16]($I_5 = 1.52 \text{ mm/min}$, 5 min 瞬时雨量为 7.6 mm, $I_{10} = 1.05 \text{ mm/min}$, 10 min 瞬时雨量为 10.6 mm),设计降雨强度分别为 60、90 mm/h(1.0、1.5 mm/min),降雨历时 90 min。由于 15° 是黄土坡面细沟发生的临界坡度,因此本研究设计的坡度为 15°。本试验中每个试验处理重复 2 次,所有数据取 2 次重复试验的平均值。

1.3 试验步骤

(1) 试验土槽底部铺 5 cm 厚细沙,细沙之上采用分层填装的方法装填黄绵土,各土层厚度为 5 cm。具体为:在试验土槽底部的细沙层上模拟当地犁底层,按 1.35 g/cm^3 的土壤容重装填黄绵土,填土厚度为 15 cm。犁底层上模拟当地耕层,按 1.10 g/cm^3 土壤容重装填黄绵土,填土厚度为 20 cm。在整个装填过程中,在装上层土之前,先将下层土的表面耕

松、打毛,以减少土壤分层现象。

(2)为保证试验前期土壤条件的一致性,正式降雨的前一天采用 30 mm/h 降雨强度进行预降雨至坡面产流为止。预降雨结束后,为防止试验土槽土壤水分蒸发,用塑料布覆盖试验土槽,静置 24 h 后进行正式试验。

(3)正式降雨开始前,随机选择一侧土槽对降雨强度进行率定,同时将另一侧土槽用塑料布覆盖,当率定值与目标降雨强度的差值小于 5% 时方可进行正式降雨试验。

(4)正式降雨开始后即仔细观察坡面产流情况,记录初始产流时间并连续接取径流样,待坡面产流稳定后每隔 2 min 收集径流样。试验过程中,在每米坡长内分别选取典型细沟 2 条和细沟间位置 2 处(若遇到坡段无细沟、细沟条数较少或坡面破碎已无较完整的细沟间位置,则减少相应的观测),分别用染色剂示踪法测量细沟间水流和细沟流的表层流速,测流区长度为 50 cm(若测距不足则改为 30 cm),同时用精度为 0.1 mm 的 SX40-1 型水位测针^[17]测量水深,所有测量均重复 2 次。

(5)坡面细沟形态的动态观测。在整个降雨过程中,大约每隔 10 min 降雨历时暂停降雨一次,待坡面退水结束后,在距离坡面前端 3 m 的 5 m 高空用三维激光扫描仪(Leica scan station 2)扫描试验土槽,获取坡面细沟高程信息。确定的扫描精度为 2 mm(水平精度)× 2 mm(垂直精度),整个扫描过程大约需要 4.5 min(包括坡面退水时间 2 min 和扫描仪工作时间 2.5 min)。同时在整个试验过程用高清照相机进行拍照记录。

(6)降雨结束后,去除径流样上层清液,然后放入干燥箱(105℃),干燥后称量,计算径流量和泥沙量。

1.4 参数计算

坡面侵蚀过程实质上是水流做功、能量不断消耗的过程,因此,本文选用径流剪切力(τ)、径流功率(ω)和单位径流功率(φ)3 个水动力学参数来描述两种降雨强度条件下总侵蚀量和细沟侵蚀量的时空分布特征。

径流剪切力是破坏和分散土壤颗粒的主要动力,其计算公式^[9]为

$$\tau = \gamma RJ \quad (1)$$

其中 $R = Bh / (B + 2h)$

式中 τ ——径流剪切力, Pa

γ ——水的容重, g/cm³

R ——水力半径, cm

J ——水力坡度, m/m, 可用土槽坡度的正切值代替^[18]

B ——径流宽度, cm

h ——径流深度, cm

BAGNOLD^[19]认为径流功率和径流剪切力存在显著的相关关系,二者的关系表达为

$$\omega = \tau V \quad (2)$$

式中 ω ——径流功率, N/(cm·s)

V ——断面平均水流流速, cm/s, 其值等于试验中测得的表层径流最大流速乘以流速修正系数 0.75^[20]

基于前人的研究结果和大量的实验数据, YANG^[21]提出了适用于明渠水流的单位径流功率的计算公式,而 MOORE 等^[22]随后用该公式进行了坡面和细沟侵蚀率的计算,结果表明该公式能够较准确地预测坡面和细沟流输沙率。在长度为 x 、总落差为 y 的一条明渠上,单位质量的水体所具备的用于输送水和泥沙的功率为

$$\varphi = \frac{dy}{dt} = \frac{dx}{dt} \frac{dy}{dx} = VJ \quad (3)$$

式中 φ ——单位径流功率, cm/s

1.5 数据处理

(1)试验结束后,首先在 Cyclone 6.0 软件里将扫描后的点云数据进行坐标系校正、拼接,为消除雨滴反射和沟壁遮挡的影响,进行降噪和插补处理,然后进行点云的抽稀并设置 X 、 Y 、 Z 坐标属性和导出精度,导出 '.txt' 格式的三维点坐标数据。

(2)将三维点坐标数据导入 ArcGIS 10.1 软件,添加 x 、 y 事件图层,创建 Tin,生成差值 Shape,然后用编辑器进行空间校准,用校准后的坡面离散点云数据再次生成 Tin,而后创建降雨前原始坡面 and 不同降雨历时下坡面的高精度 DEM 数据(精度为 5 mm×5 mm),通过 3D 分析模块,运用表面体积、填挖方、表面差异等子模块计算细沟体积和沉降体积的时空分布。

(3)以与水平面平行且通过三维激光扫描仪激光源的平面为参考平面,分别计算不同时期 DEM 与参考平面 DEM 围成的体积,通过前后两期 DEM 相减,获取细沟体积差值,乘以坡面土壤容重,即可得到不同降雨历时下的细沟侵蚀量。

2 结果与讨论

2.1 不同降雨强度下的总侵蚀量和细沟侵蚀量

细沟发育不同阶段的主导侵蚀方式有明显差异。本研究将细沟侵蚀的 3 个子过程进行如下划分:以沟头溯源侵蚀为主的阶段出现在细沟发育初期,从跌水形成时起至断续细沟连接形成连续细沟时止;以细沟沟底下切侵蚀为主的阶段出现在细沟

发育中期,从连续细沟形成固定流路时起至细沟底部下切至犁底层(细沟深度为 20 cm)时止;以沟壁崩塌侵蚀为主的阶段出现在细沟发育末期,此时细沟沟槽已切入犁底层,细沟深度大于 20 cm,下切侵蚀速率降低,侵蚀方式以细沟沟壁崩塌为主。

由于细沟发育不同阶段的主导侵蚀方式不同,所以细沟侵蚀速率、总侵蚀速率以及细沟侵蚀量对总侵蚀量的贡献亦不相同。表 1 表明,试验条件下,90 mm/h 降雨强度下以沟头溯源侵蚀为主的侵蚀方式持续的时间为 30 min,较 60 mm/h 降雨强度条件下短 10 min;两种降雨强度条件下以细沟下切侵蚀为主的侵蚀方式持续时间相同,均为 30 min;90 mm/h 降雨强度下以沟壁崩塌侵蚀为主的侵蚀方式开始时间为 60 min,较 60 mm/h 降雨强度条件提前 10 min。随着主导侵蚀方式由沟头溯源侵蚀演变为沟壁崩塌侵蚀,2 种降雨强度条件下的细沟侵蚀速率和总侵蚀速率的最大值出现在以细沟下切侵蚀为主并伴随沟壁崩塌侵蚀的发育活跃期,而细沟侵蚀量对总侵蚀量的贡献率则一直呈增大趋势。出现上述现象的主要原因为:①以沟头溯源侵蚀为主的阶段,坡面中下部是土壤抗蚀性相对较弱的坡段,其径流剪切力大于土壤的临界抗剪强度^[23],首先形成断续的跌水,跌水逐渐连接形成断续细沟,细沟沟头溯源侵蚀逐渐连接成为连续细沟,形成固定流路和微小流域(图 1a、1d)。此时坡面破碎程度相对较低,坡面上以细沟间水流为主,流速慢,侵蚀力相对较弱,而细沟流也因大面积细沟间水流的存在,流量小,流速慢,径流剪切力低,侵蚀能力较后两阶段弱,所

以细沟侵蚀速率较小,60 mm/h、90 mm/h 降雨强度下的细沟侵蚀速率分别为 8.3 kg/(m²·h)和 22.8 kg/(m²·h),仅相当于最大细沟侵蚀速率的 1/3 和 1/2,坡面总侵蚀速率和细沟侵蚀量对总侵蚀量的贡献亦较小。②以细沟沟底下切侵蚀为主并伴随沟壁崩塌侵蚀的阶段是坡面细沟发育最活跃的时期,此时沟头溯源侵蚀已基本停止,沟头位置接近分水岭(试验土槽的上边缘),坡面进一步破碎,细沟间水流流速降低,大部分径流汇入细沟成为沟内股流,由于沟内股流流速快、流量大,径流剪切力和径流功率远大于细沟间水流,使细沟沟底进一步加深,流路进一步明确,同时,该阶段还伴随着细沟沟壁的横向扩张,但沟壁崩塌侵蚀并不是该阶段细沟侵蚀量增大的主要因素(图 1b、1e)。③以沟壁崩塌侵蚀为主的阶段存在于细沟发育的末期,这与 BRUNTON 等^[23]对加拿大黄土坡面的研究结果类似,该研究认为试验条件下,坡面细沟出现崩塌侵蚀的时间比出现下切侵蚀的时间晚 36~52 min,该阶段细沟发育逐渐趋于稳定,由于沟头溯源侵蚀和细沟下切侵蚀均已停止,坡面产沙主要来源于沟壁崩塌,坡面形态较上一阶段更加破碎(图 1c、1f),细沟间水流所引起的细沟间侵蚀相对较小,所以细沟侵蚀量对总侵蚀量的贡献率最大(2 种降雨强度下均大于 75%),但由于沟壁崩塌具有不确定性和突发性等特点,且坡面可被侵蚀的物质逐渐减少,故 90 mm/h 降雨强度下的细沟侵蚀速率和总侵蚀速率小于以细沟下切侵蚀为主并伴随沟壁崩塌侵蚀的阶段。

表 1 细沟发育不同主导过程的细沟侵蚀速率、总侵蚀速率和细沟侵蚀量对总侵蚀量的贡献率

Tab. 1 Rill erosion rate, hillslope erosion rate and contribution of rill erosion to hillslope erosion at different dominated process of rill development

降雨强度/ (mm·h ⁻¹)	主导侵蚀方式	降雨历时/ min	细沟侵蚀速率/ (kg·m ⁻² ·h ⁻¹)	总侵蚀速率/ (kg·m ⁻² ·h ⁻¹)	细沟侵蚀量对总 侵蚀量的贡献率/%
60	沟头溯源侵蚀	0~40	8.3	22.4	37.1
	细沟下切侵蚀	40~70	24.3	31.9	76.2
	沟壁崩塌侵蚀	70~90	24.2	31.6	76.5
90	沟头溯源侵蚀	0~30	22.8	42.7	53.4
	细沟下切侵蚀	30~60	48.0	61.6	77.8
	沟壁崩塌侵蚀	60~90	40.8	50.7	80.5

2.2 细沟侵蚀的时空变化

2.2.1 细沟侵蚀随时间的变化特征

60 mm/h、90 mm/h 降雨强度下的坡面总侵蚀量分别为 621.3 kg、1 162.5 kg,细沟侵蚀量分别为 386.3 kg、837.0 kg,细沟侵蚀量对总侵蚀量的贡献率分别为 62.2%、72.0%(图 2)。相同的降雨强度条件下,总侵蚀速率达到峰值的时间早于细沟侵蚀

速率;较大的降雨强度可使总侵蚀速率和细沟侵蚀速率较早地达到峰值。具体来说,60 mm/h 降雨强度条件下,总侵蚀速率和细沟侵蚀速率达到峰值的时间分别为 40 min、60 min,达到峰值后分别在 30.6~32.9 kg/(m²·h)和 23.6~26.8 kg/(m²·h)范围内波动;90 mm/h 降雨强度条件下,总侵蚀速率和细沟侵蚀速率达到峰值的时间分别为 30 min、40 min,分

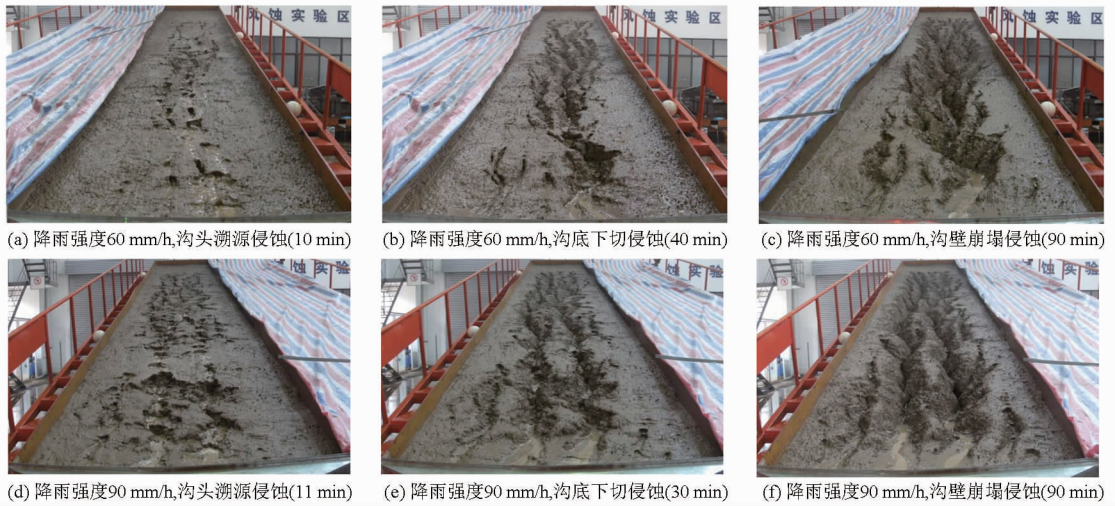


图1 细沟发育不同阶段的主导侵蚀方式

Fig. 1 Dominated erosion patterns at different stages of rill development process

别较前者提前 10 min、20 min, 达到峰值后分别在 47.7 ~ 67.0 kg/(m²·h) 和 37.7 ~ 45.7 kg/(m²·h) 范围内波动, 这与 BERGER 等^[24] 的研究结论类似, 该研究认为随着降雨强度的增加, 细沟发育达到稳定的时间亦随之提前。分析原因是, 试验条件下 90 mm/h 降雨强度具有较强的雨滴动能并能产生较大的汇流强度, 雨滴击溅侵蚀和径流侵蚀能力较强, 坡面侵蚀过程较 60 mm/h 降雨强度迅速, 细沟发育达到稳定阶段, 即侵蚀方式进入以沟壁崩塌为主的时间较 60 mm/h 降雨强度提前。此外, 细沟侵蚀量对总侵蚀量贡献率的峰值也在 90 mm/h 降雨强度下较早达到, 2 种降雨强度下, 细沟侵蚀量对总侵蚀量的贡献率达到峰值后, 均呈稳定并小幅波动的趋势, 波动范围差别不大, 介于 72.6% ~ 81.5%, 这符合前人对黄土高原细沟侵蚀区研究的有关结论^[1-2], 即细沟侵蚀量占坡面总侵蚀量的 70% 左右。

2.2.2 细沟侵蚀随单位坡长的变化特征

2 种降雨强度下的细沟侵蚀速率随单位斜坡长

均呈先上升后下降的抛物线形式分布(图 3)。从细沟发育的不同阶段来看, 以细沟下切侵蚀为主并伴随沟壁崩塌侵蚀阶段的细沟侵蚀速率最大, 以沟头溯源侵蚀为主的阶段细沟侵蚀速率最小(表 1、图 2); 从不同坡位来看, 坡面中下部(斜坡长 6、7 m 处)的细沟侵蚀速率较其它坡位的细沟侵蚀速率大(图 3)。

具体来说, 60 mm/h 降雨强度下, 0 ~ 90 min 降雨历时的坡面平均细沟侵蚀速率随斜坡长变化的分布曲线介于 0 ~ 40 min 和 70 ~ 90 min 降雨历时的曲线之间, 最大值出现在斜坡长 7 m 处, 其值为 33.1 kg/(m²·h), 是坡面平均值的 3.3 倍, 这与前人的研究结果, 坡面侵蚀的强烈区域位于坡面的中下部的结论相一致^[25-26]。在细沟发育的初期(0 ~ 40 min), 侵蚀方式以沟头溯源侵蚀为主, 细沟侵蚀速率随斜坡长的分布曲线较缓, 除坡顶和坡脚处外, 其余坡位的细沟侵蚀速率差别相对较小。在细沟发育的中期(40 ~ 70 min), 侵蚀方式以细沟下切侵蚀为主, 同时伴随沟壁崩塌侵蚀, 斜坡长 5 ~ 8 m 处的

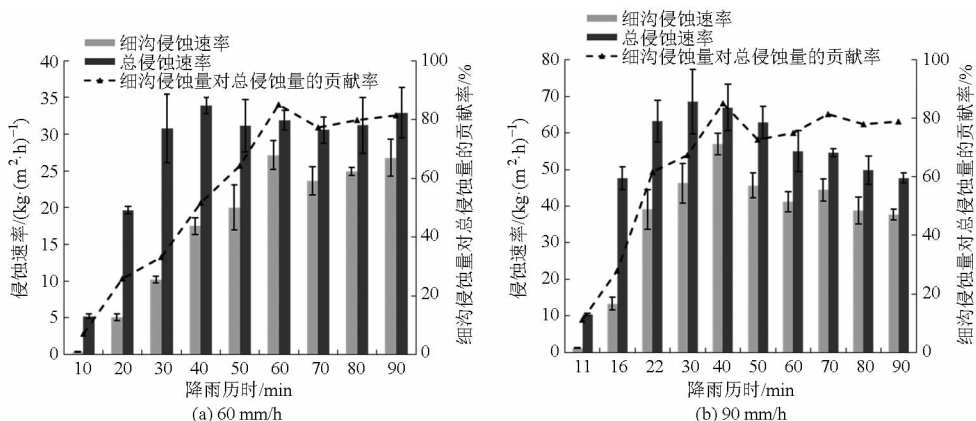


图2 不同降雨历时下的细沟侵蚀速率、总侵蚀速率和细沟侵蚀量对总侵蚀量的贡献

Fig. 2 Rill erosion rate, hillslope erosion rate and contribution of rill erosion to hillslope erosion under different rainfall durations

细沟侵蚀速率明显大于其它细沟发育阶段,该阶段是细沟发育最活跃的时期,该阶段过后,细沟发育逐渐趋于稳定,主细沟沟底下切至犁底层,下切侵蚀过程结束。在细沟发育的末期(70~90 min),坡面中上部(斜坡长 1~5 m)细沟侵蚀速率的绝对值与前一阶段基本相同,但坡面中下部(斜坡长 6~9 m)的细沟侵蚀速率明显降低,降低幅度介于 13.9%~31.7%。分析原因主要为,本阶段坡面中上部的细沟深度相对较浅,细沟沟底尚未下切至犁底层,细沟下切侵蚀和沟壁崩塌侵蚀两种侵蚀方式并存,而坡面中下部的细沟下切侵蚀过程已经结束,细沟侵蚀量主要来源于随机性较强的沟壁崩塌侵蚀,因此侵蚀速率明显降低。90 mm/h 降雨强度下,细沟发育不同阶段细沟侵蚀速率随单位斜坡长的分布规律与 60 mm/h 降雨强度下的基本一致,细沟侵蚀速率的坡面平均值是 60 mm/h 降雨强度下的 1.8~2.8 倍。但在细沟发育的末期(60~90 min),与 60 mm/h 降雨强度细沟侵蚀速率从斜坡长 6 m 处开始降低不同,90 mm/h 降雨强度下细沟侵蚀速率从斜坡长 4 m 处即开始降低。其原因与 4 m 斜坡长处部分细沟下切至犁底层有关。

结合三维激光扫描数据,分析可知两种降雨强度下 1~7 m 斜坡长坡面以侵蚀和搬运过程为主。受汇水坡长限制,坡面上部的径流剪切力和径流功率均小于坡面中下部(图 4),导致其细沟侵蚀速率也小于坡面中下部的细沟侵蚀速率,特别是在斜坡长 1 m 处,坡面侵蚀以细沟间侵蚀为主,60 mm/h、90 mm/h 降雨强度下的平均细沟侵蚀速率仅分别为 0.2 kg/(m²·h)、3.7 kg/(m²·h)(图 3)。随着坡长的加长,汇水面积增大,径流的剥蚀能力逐渐增强,径流功率和单位径流功率亦增大(图 4)。在细沟侵蚀速率达到峰值后,其值逐渐降低,但降低程度不明显,该坡段(斜坡长 8、9 m)的坡面侵蚀、搬运、沉积 3 个过程并存,且沉积过程占主导,这与吴普特等^[26]有关径流搬运能力的论述相吻合;在斜坡长 10 m 处,由于临近出水口,两种降雨强度下的细沟侵蚀速率显著降低,点云数据生成的高精度 DEM 和试验照片均表明该坡段以沉积过程为主,细沟内淤积明显,且多发育‘宽浅’型细沟,与坡面中上部发育的‘窄深’型细沟不同(图 1),这与野外发育在梁峁坡上直接汇入沟坡的细沟沉积情况类似,也符合 BRUNTON 等^[23]得到的黄土坡面细沟沿坡长的分布规律。

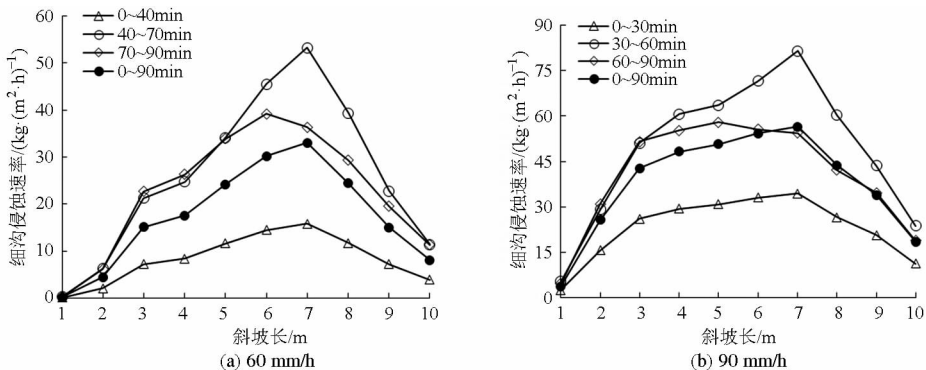


图 3 细沟发育不同阶段细沟侵蚀速率随单位斜坡长的变化曲线

Fig. 3 Changes of rill erosion rate with unit hillslope length at different stages of rill development process

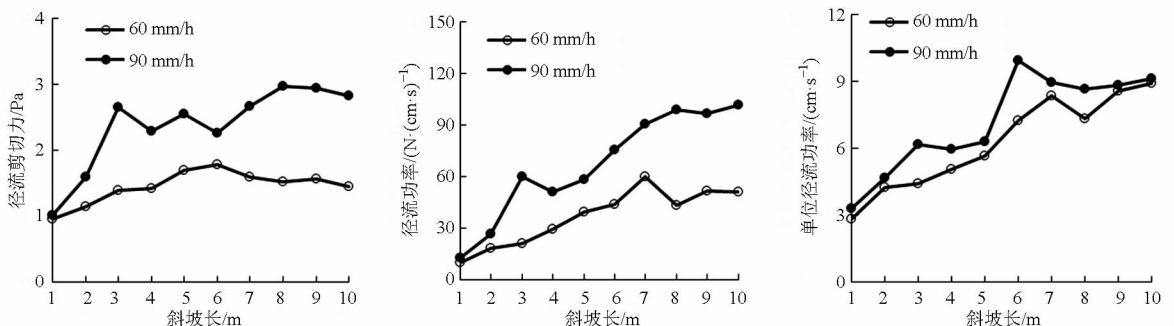


图 4 径流剪切力、径流功率和单位径流功率随单位斜坡长的变化曲线

Fig. 4 Changes of shear stress, stream power and unit stream power with unit hillslope length

2.3 水动力学参数的时空变化

2.3.1 水动力学参数随时间的变化特征

从不同降雨强度来看,90 mm/h 降雨强度下径流剪切力、径流功率和单位径流功率均明显大于

60 mm/h 降雨强度,且前者分别是后者的 1.3 倍、1.1 倍和 1.4 倍(表 2)。从水动力学参数在细沟发育不同阶段的变化情况来看,随坡面主导侵蚀方式由溯源侵蚀为主向崩塌侵蚀为主转变,2 种降雨强

度下的径流剪切力、径流功率和单位径流功率的坡面平均值均呈下降趋势。但细沟间水流和细沟流由于流速、流态等的差异,3个水动力学参数随细沟发育过程的变化情况有所不同,这印证了坡面侵蚀方式的转变可显著影响坡面流体力学特性这一研究成果^[27]。具体来说,2种降雨强度下细沟间水流的水动力学参数随降雨的进行呈下降趋势,而细沟流的水动力学参数则随降雨历时的增加呈先上升后下降的趋势。分析原因主要是:①以沟头溯源侵蚀为主的细沟发育初期,坡面相对完整,大部分坡面流以细沟间水流形式存在,细沟流相对较少;随着细沟的发育,细沟网形成,径

流集中程度增加,细沟间水流的汇流面积减少,流量、流速均大幅降低,大部分细沟间水流最终汇入细沟,细沟成为输送径流泥沙的通道,此时细沟间水流的径流剪切力、径流功率和单位径流功率随之下落。②与细沟间水流相反,随着流路的形成、细沟的发育和径流的汇集,细沟流的水动力学参数逐渐增大,但随着沟壁崩塌侵蚀成为坡面侵蚀的主要方式,其随机性和不确定性导致崩塌物在细沟沟槽内的不定时堆积,进而降低了径流流速,增加了径流的流深和流宽,使以沟壁崩塌侵蚀为主的阶段,细沟流的水动力学参数小于以沟底下切侵蚀为主的细沟发育阶段。

表2 细沟发育不同阶段细沟间水流和细沟流的径流剪切力、径流功率和单位径流功率

Tab.2 Shear stress, stream power and unit stream power of inter-rill flow and rill flow at different stages of rill development process

降雨强度/(mm·h ⁻¹)	主导侵蚀方式	降雨历时/min	径流类型	τ /Pa	ω /(N·cm ⁻¹ ·s ⁻¹)	φ /(cm·s ⁻¹)
60	沟头溯源侵蚀	0~40	细沟间水流	1.3	25.4	6.0
			细沟流	2.1	63.5	7.9
	细沟下切侵蚀	40~70	细沟间水流	1.0	13.5	3.4
			细沟流	2.2	69.5	7.9
	沟壁崩塌侵蚀	70~90	细沟间水流	0.8	12.3	3.1
			细沟流	1.7	55.5	7.7
90	沟头溯源侵蚀	0~30	细沟间水流	1.6	41.4	6.3
			细沟流	2.8	85.9	8.5
	细沟下切侵蚀	30~60	细沟间水流	1.2	16.9	3.9
			细沟流	3.1	95.3	9.1
	沟壁崩塌侵蚀	60~90	细沟间水流	1.1	15.4	3.6
			细沟流	2.5	82.8	8.7

2.3.2 水动力学参数随单位坡长的变化特征

从水动力学参数随单位斜坡长的变化情况来看,2种降雨强度下,径流剪切力、径流功率和单位径流功率随单位坡长的分布均呈波动上升趋势(图4)。90 mm/h降雨强度下3个水动力学参数的波动更加明显,主要原因为较大的降雨强度增加了细沟发育过程的随机性和不确定性,集中股流的冲刷力更强,使沟头溯源侵蚀和沟壁崩塌侵蚀过程中的掏刷作用更加强烈。实测资料表明,以沟头溯源侵蚀为主的阶段,90 mm/h降雨强度下细沟沟头内凹的平均深度是3.5 cm,较60 mm/h降雨强度下深1.3 cm,有关研究证实^[28],在一定范围内,上方汇流强度与沟头土体内凹深度呈正相关关系;以沟壁崩塌侵蚀为主的阶段,90 mm/h降雨强度下细沟沟壁掏刷的平均深度是4.2 cm,较60 mm/h降雨强度下深1.5 cm。较大的掏刷深度使悬空土体的体积增加,不稳定土体的自重增大,崩塌侵蚀的不确定性增强,最终影响径流的流速和流态,从而引起3个水动力学参数的沿程波动,WELLS等^[28]有关沟头溯源侵蚀的研究

则指出,沟头土体内凹深度越大,溯源侵蚀速率也越大。在斜坡长0~7 m处,3个水动力学参数沿单位坡长的变化趋势与细沟侵蚀速率随单位坡长的变化趋势基本一致,细沟侵蚀速率随径流剪切力、径流功率和单位径流功率的增大而增大。但在斜坡长7~10 m处,细沟侵蚀速率随单位坡长的变化趋势与径流剪切力、径流功率和单位径流功率随单位坡长的变化趋势相反,细沟侵蚀速率随3个水动力学参数的增大而减小,这主要与径流的挟沙能力以及坡面由以侵蚀过程为主向以沉积过程为主的转变有关^[23]。

2.4 细沟侵蚀量与水动力学参数的关系

为进一步阐明细沟侵蚀量与水动力学参数之间的关系,将两种降雨强度下细沟不同发育阶段的单宽细沟侵蚀量与径流剪切力、径流功率和单位径流功率进行回归分析,方程拟合。拟合时仅选取斜坡长2~7 m处的细沟侵蚀量和水动力学参数进行计算,主要原因为:斜坡长1 m处的主要侵蚀方式是片蚀;斜坡长8~10 m处有沉积发生,故而剔除了以上

2 个坡段的数据。

由表 3 可知,单宽细沟侵蚀量 D_c ($\text{kg}/(\text{h}\cdot\text{m})$) 与水动力学参数呈线性相关关系且所有拟合方程的决定系数均大于 0.6,说明细沟侵蚀量与水动力学参数之间有较好的线性相关性。具体来看,拟合方程的一次项系数在以细沟下切侵蚀为主的细沟发育阶段最大,表明该阶段拟合直线的斜率最大,即在水动力学参数增加量一致的情况下,单宽细沟侵蚀量增加最快,这与该阶段细沟侵蚀速率和总侵蚀速率均达到最大值一致。坡面流克服土壤颗粒之间的粘结力做功使土壤颗粒恰好发生位移时的径流剪切力、径流功率和单位径流功率即为坡面侵蚀发生的临界径流剪切力、临界径流功率和临界单位径流功率,由表 3 所述关系式可知,当单宽细沟侵蚀量 D_c 为零时,对应得到的常数项数值即为使坡面侵蚀发生的水动力学参数临界值。在以沟头溯源侵蚀为主的发育初期,使坡面侵蚀发生的临界径流剪切力、临界径流功率和临界单位径流功率最大,分别为 0.748 Pa、1.319 $\text{N}/(\text{cm}\cdot\text{s})$ 和 1.504 cm/s 。随着细沟的发育,发生侵蚀的临界径流剪切力、临界径流功率和临界单位径流功率逐渐降低,在以崩塌侵蚀为

主的发育末期,临界径流剪切力、临界径流功率和临界单位径流功率分别仅为在以沟头溯源侵蚀为主的发育初期的 48.6%、62.6%、50.1%。分析原因,主要为:①试验前期的预降雨使坡面产生了一层相对致密的土壤结皮,从而使坡面流剥蚀土壤所需的能量最大,这与 AN 等^[29]基于黑土坡面的研究结果类似。②在第 2 阶段,由于大部分的土壤结皮已被破坏,且坡面径流主要以细沟股流的形式存在,径流流量大,流速快,侵蚀能力急剧上升,所以使侵蚀发生的临界能量比第一阶段小。③在第 3 阶段,坡面侵蚀产沙主要来源于细沟沟壁的不定时崩塌,由于股流对沟壁的淘涮作用,使沟壁形成上下窄、中间宽的菱形横断面(图 1f 中下部),当沟壁土体自身重力大于土粒间的粘结力时,沟壁随即崩塌,崩塌形式与 WELLS 等^[30]对美国密西西比地区坡面沟壁崩塌侵蚀研究的结论类似,崩塌物堆积在细沟沟槽内并被股流搬运至出水口产沙。由于沟壁崩塌侵蚀是水力侵蚀和重力侵蚀共同作用的结果,因此单宽细沟侵蚀量与水力学性质关系逐渐降低,引起细沟侵蚀的随机性变强,临界径流剪切力、临界径流功率和临界单位径流功率降低。

表 3 细沟发育不同阶段单宽细沟侵蚀量与水动力学参数的拟合方程

Tab.3 Fitted equations between rill erosion per unit width and hydrodynamic parameters at different stages of rill development process

主导侵蚀 方式	τ			ω			φ		
	拟合方程	样本数	R^2	拟合方程	样本数	R^2	拟合方程	样本数	R^2
溯源侵蚀	$D_c = 54.97(\tau - 0.748)$	14	0.85	$D_c = 1.262(\omega - 1.319)$	14	0.68	$D_c = 11.29(\varphi - 0.015)$	14	0.63
下切侵蚀	$D_c = 82.61(\tau - 0.675)$	14	0.82	$D_c = 2.131(\omega - 1.075)$	14	0.82	$D_c = 21.01(\varphi - 0.012)$	14	0.62
崩塌侵蚀	$D_c = 50.44(\tau - 0.364)$	14	0.66	$D_c = 1.763(\omega - 0.827)$	14	0.74	$D_c = 14.12(\varphi - 0.007)$	14	0.63

3 结论

(1) 90 mm/h 降雨强度下的坡面总侵蚀量、细沟侵蚀量和细沟侵蚀量对总侵蚀量的贡献率分别是 60 mm/h 降雨强度下的 1.9、2.2、1.2 倍;90 mm/h 降雨强度下总侵蚀速率、细沟侵蚀速率和细沟侵蚀量对总侵蚀量贡献率达到峰值的时间早于 60 mm/h 降雨强度。

(2) 细沟侵蚀速率和总侵蚀速率的最大值均出现在以细沟沟底下切侵蚀为主并伴随沟壁崩塌侵蚀的阶段;细沟侵蚀速率和总侵蚀速率的最小值出现在以沟头溯源侵蚀为主的阶段;从不同坡位来看,细沟侵蚀速率随单位斜坡长呈先上升后下降的抛物

线形式分布,坡面中下部的细沟侵蚀速率较其它坡位的细沟侵蚀速率大。

(3) 90 mm/h 降雨强度下的径流剪切力、径流功率和单位径流功率分别是 60 mm/h 降雨强度下的 1.3、1.1、1.4 倍。细沟间水流的水动力学参数随细沟的发育呈下降趋势,而细沟流的水动力学参数则随细沟的发育呈先上升后下降的趋势。

(4) 细沟发育初期使坡面侵蚀发生的临界径流剪切力、临界径流功率和临界单位径流功率最大;在细沟发育末期,主导侵蚀方式为沟壁崩塌侵蚀,临界径流剪切力、临界径流功率和临界单位径流功率最小。

参 考 文 献

1 朱显谟. 黄土高原水蚀的主要类型及其有关因素[J]. 水土保持通报, 1982(1): 1-9.

ZHU Xianmo. Main water erosion types and their related factors in the Loess Plateau [J]. Bulletin of Soil and Water Conservation,

- 1982(1): 1-9. (in Chinese)
- 2 郑粉莉, 唐克丽, 周佩华. 坡耕地细沟侵蚀影响因素的研究[J]. 土壤学报, 1989, 26(2): 109-116.
ZHENG Fenli, TANG Keli, ZHOU Peihua. Study on factors affecting rill erosion on cultivated slope land [J]. Acta Pedologica Sinica, 1989, 26(2): 109-116. (in Chinese)
- 3 李君兰, 蔡强国, 孙莉英, 等. 细沟侵蚀影响因素和临界条件研究进展[J]. 地理科学进展, 2010, 29(11): 1319-1325.
LI Junlan, CAI Qiangguo, SUN Liying, et al. Reviewing on factors and critical conditions of rill erosion [J]. Process in Geography, 2010, 29(11): 1319-1325. (in Chinese)
- 4 ZHENG F L, TANG K L. Rill erosion process on steep slope land of the Loess Plateau [J]. International Journal of Sediment Research, 1997, 12(1): 52-59.
- 5 ELLIOT W J, LAFLEN J M. A process-based rill erosion model [J]. Transactions of the ASAE, 1993, 36(1): 65-72.
- 6 沈海鸥, 郑粉莉, 温磊磊, 等. 降雨强度和坡度对细沟形态特征的综合影响[J]. 农业机械学报, 2015, 46(7): 162-170.
SHEN Haiou, ZHENG Fenli, WEN Leilei, et al. Effects of rainfall intensity and slope gradient on rill morphological characteristics [J]. Transactions of the Chinese Society for Agricultural Machinery, 2015, 46(7): 162-170. (in Chinese)
- 7 张永东, 吴淑芳, 冯浩, 等. 黄土陡坡细沟侵蚀动态发育过程及其发生临界动力条件试验研究[J]. 泥沙研究, 2013(2): 25-32.
ZHANG Yongdong, WU Shufang, FENG Hao, et al. Experimental study of rill dynamic development process and its critical dynamic conditions on loess slope [J]. Journal of Sediment Research, 2013(2): 25-32. (in Chinese)
- 8 李鹏, 李占斌, 郑良勇. 黄土陡坡径流侵蚀产沙特性室内实验研究[J]. 农业工程学报, 2005, 21(7): 42-45.
LI Peng, LI Zhanbin, ZHENG Liangyong. Indoor experiment of characteristics of runoff erosion in loess steep slope [J]. Transactions of the CSAE, 2005, 21(7): 42-45. (in Chinese)
- 9 FOSTER G R, HUGGINS L F, MEYER L D. A laboratory study of rill hydraulics; II. shear stress relationships [J]. Transactions of the ASAE, 1984, 27(3): 797-804.
- 10 韩鹏, 倪晋仁, 李天宏. 细沟发育过程中的溯源侵蚀与沟壁崩塌[J]. 应用基础与工程科学学报, 2002, 10(2): 115-125.
HAN Peng, NI Jinren, LI Tianhong. Headcut and bank landslip in rill evolution [J]. Journal of Basic Science and Engineering, 2002, 10(2): 115-125. (in Chinese)
- 11 MEYER L D, FORSTER G R, NIKOLOVE S. Effect of flow rate and canopy on rill erosion [J]. Transactions of the ASAE, 1975, 18(5): 905-911.
- 12 LYLE W M, SMERDEN E T. Relation of compaction and other soil prosperities to erosion resistance of soils [J]. Transactions of ASAE, 1965, 8: 419-422.
- 13 NEARING M A, BRADFORD J M, PARKER S C. Soil detachment by shallow flow at low slopes [J]. Soil Science Society of American Journal, 1991, 55(2): 339-344.
- 14 NEARING M A, FOSTER G R, LANE L J, et al. A process based soil erosion model for USDA—water erosion prediction project technology [J]. Transactions of the ASAE, 1989, 32(5): 1587-1593.
- 15 郑粉莉, 赵军. 人工模拟降雨大厅及模拟降雨设备简介 [J]. 水土保持研究, 2004, 11(4): 177-178.
ZHENG Fenli, ZHAO Jun. Introduction of the artificial rainfall simulation hall and simulated rainfall equipment [J]. Research of Soil and Water Conservation, 2004, 11(4): 177-178. (in Chinese)
- 16 周佩华, 王占礼. 黄土高原土壤侵蚀暴雨标准 [J]. 水土保持通报, 1987, 7(1): 38-44.
ZHOU Peihua, WANG Zhanli. Soil erosion storm rainfall standard in the Loess Plateau [J]. Bulletin of Soil and Water Conservation, 1987, 7(1): 38-44. (in Chinese)
- 17 施明新, 李陶陶, 吴秉校, 等. 地表粗糙度对坡面流水动力学参数的影响 [J]. 泥沙研究, 2015(4): 59-65.
SHI Mingxin, LI Taotao, WU Bingxiao, et al. Influences of surface roughness on overland flow hydraulic characteristics [J]. Journal of Sediment Reasesrch, 2015(4): 59-65. (in Chinese)
- 18 ZHU J C, GANTZER C J, ANDERSON S H, et al. Simulated small-channel bed scour and head cut erosion rates compared [J]. Soil Science Society of America Journal, 1995, 59(1): 211-218.
- 19 BAGNOLD R A. An approach to the sediment transport problem for general physics [M]. Washington: United States Government Printing Office, 1966: 5.
- 20 沈海鸥, 郑粉莉, 温磊磊, 等. 雨滴打击对黄土坡面细沟侵蚀特征的影响 [J]. 农业机械学报, 2015, 46(8): 104-112, 89.
SHEN Haiou, ZHENG Fenli, WEN Leilei, et al. Effects of raindrop impact on rill erosion characteristics on Loess Hillslope [J]. Transactions of the Chinese Society for Agricultural Machinery, 2015, 46(8): 104-112, 89. (in Chinese)
- 21 YANG C T. Incipient motion and sediment transport [J]. Journal of the Hydraulics Division, 1973, 99(10): 1679-1704.
- 22 MOORE I D, BURCH G J. Sediment transport capacity of sheet and rill flow: application of unit stream power theory [J]. Water Resources Research, 1986, 22(8): 1350-1360.
- 23 BRUNTON D A, BRYAN R B. Rill network development and sediment budgets [J]. Earth Surface Processes and Landforms, 2000, 25(7): 783-800.
- 24 BERGER C, SCHULZE M, RIEKE-ZAPP D, et al. Rill development and soil erosion: a laboratory study of slope and rainfall intensity [J]. Earth Surface Processes and Landforms, 2010, 35(12): 1456-1467.

- SHANG Manting, FENG Jie, LIU Peigui, et al. On formulas for soil suction and optimum centrifugal time by use of SWCC[J]. Journal of Hohai University, 2009, 37(1): 12 - 15. (in Chinese)
- 14 VAN GENUCHTEN M T. A closed-form equation for predicting the hydraulic conductivity of unsaturated soils[J]. Soil Science Society of America Journal, 1980, 44(5): 892 - 898.
- 15 MUALEM Y. A new model for predicting the hydraulic conductivity of unsaturated porous media[J]. Water Resources Research, 1975, 12(3): 513 - 522.
- 16 BRUCE R R, KLUTE A. The measurement of soil moisture diffusivity[J]. Soil Science Society of America Journal, 1956, 20(4): 458 - 462.
- 17 ATANU M, RATTAN L. Biochar impacts on soil physical properties and greenhouse gas emissions[J]. Agronomy, 2013, 3(2): 313 - 339.
- 18 汪东林, 栾茂田, 杨庆. 重塑非饱和黏土的土-水特征曲线及其影响因素研究[J]. 岩土力学, 2009, 30(3): 751 - 756.
WANG Donglin, LUAN Maotian, YANG Qing. Experimental study of soil-water characteristic curve of remolded unsaturated clay [J]. Rock and Soil Mechanics, 2009, 30(3): 751 - 756. (in Chinese)
- 19 冯小江, 伊松林, 张齐生. 热解条件对农作物秸秆炭性能的影响[J]. 北京林业大学学报, 2009, 31(增刊): 182 - 184.
FENG Xiaojiang, YI Songlin, ZHANG Qisheng. Effects of pyrolysis conditions on performance of crop stalk carbon[J]. Journal of Beijing Forestry University, 2009, 31(Supp.): 182 - 184. (in Chinese)
- 20 邹文秀, 韩晓增, 江恒, 等. 东北黑土区降水特征及其对土壤水分的影响[J]. 农业工程学报, 2011, 27(9): 196 - 202.
ZOU Wenxiu, HAN Xiaozeng, JIANG Heng, et al. Characteristics of precipitation in black soil region and response of soil moisture dynamics in Northeast China[J]. Transactions of the CSAE, 2011, 27(9): 196 - 202. (in Chinese)
- 21 候月卿, 赵立欣, 孟海波, 等. 生物炭和腐植酸类对猪粪堆肥重金属的钝化效果[J]. 农业工程学报, 2014, 30(11): 205 - 215.
HOU Yueqing, ZHAO Lixin, MENG Haibo, et al. Passivating effect of biochar and humic acid materials on heavy metals during composting of pig manure[J]. Transactions of the CSAE, 2014, 30(11): 205 - 215. (in Chinese)
- 22 朱继荣, 韦绪好, 祝鹏飞, 等. 施用生物炭抑制塌陷区复垦土壤硝化作用[J]. 农业工程学报, 2015, 31(7): 264 - 271.
ZHU Jirong, WEI Xuhao, ZHU Pengfei, et al. Biochar addition inhibiting nitrification of reclaimed soils in coal-mining subsidence area[J]. Transactions of the CSAE, 2015, 31(7): 264 - 271. (in Chinese)
- 23 LAIRD D A, FLEMING P, DAVIS D D, et al. Impact of biochar amendment on the quality of a typical midwestern agricultural soil [J]. Geoderma, 2010, 158(3 - 4): 443 - 449.
- 24 王红兰, 唐翔宇, 张维, 等. 施用生物炭对紫色土坡耕地根区土壤水力学性质的影响[J]. 农业工程学报, 2015, 31(4): 107 - 112.
WANG Honglan, TANG Xiangyu, ZHANG Wei, et al. Effects of biochar application on tillage soil hydraulic properties of slope cropland of purple soil[J]. Transactions of the CSAE, 2015, 31(4): 107 - 112. (in Chinese)

(上接第 154 页)

- 25 覃超, 郑粉莉, 徐锡蒙, 等. 玉米秸秆缓冲带防治黄土坡面细沟侵蚀的效果[J]. 中国水土保持科学, 2015, 13(1): 35 - 42.
QIN Chao, ZHENG Fenli, XU Ximeng, et al. Effects of maize straw buffer in preventing rill erosion on loess slope[J]. Science of Soil and Water Conservation, 2015, 13(1): 35 - 42. (in Chinese)
- 26 吴普特, 周佩华, 武春龙, 等. 坡面细沟侵蚀垂直分布特征研究[J]. 水土保持研究, 1997, 4(2): 47 - 56.
WU Pute, ZHOU Peihua, WU Chunlong, et al. Research on the spatial distribution characteristics of slope rill erosion[J]. Research of Soil and Water Conservation, 1997, 4(2): 47 - 56. (in Chinese)
- 27 温磊磊, 郑粉莉, 沈海鸥, 等. 沟头秸秆覆盖对东北黑土区坡耕地沟蚀发育影响的试验研究[J]. 泥沙研究, 2014(6): 73 - 80.
WEN Leilei, ZHENG Fenli, SHEN Haiou, et al. Effects of corn straw mulch buffer in the gully head on gully erosion of sloping cropland in the black soil region of northeast China[J]. Journal of Sediment Research, 2014(6): 73 - 80. (in Chinese)
- 28 WELLS R R, BENNETT S J, ALONSO C V. Modulation of headcut soil erosion in rills due to upstream sediment loads[J]. Water Resources Research, 2010, 46(12): 1 - 16.
- 29 AN J, ZHENG F L, LU J, et al. Investigating the role of raindrop impact on hydrodynamic mechanism of soil erosion under simulated rainfall conditions[J]. Soil Science, 2012, 177(8): 517 - 526.
- 30 WELLS R R, MOMM H G, RIGBY J R, et al. An empirical investigation of gully widening rates in upland concentrated flows [J]. CATENA, 2013, 101: 114 - 121.